Linear Quadrupoles with Added Hexapole Fields

Nikolai Konenkov
Department of General Physics, Ryazan State Pedagogical University, Ryazan, Russia

Frank Londry
Pan Galactic Scientific, Omemee, Ontario, Canada

Chuanfan Ding* and D. J. Douglas
Department of Chemistry, University of British Columbia, Vancouver, British Columbia, Canada

Linear quadrupoles with added hexapole fields are described. The shifts in ion oscillation frequency caused by the addition of a hexapole field are calculated within the effective potential model. Methods to construct linear quadrupoles with added hexapole fields with exact electrode geometries and with round rods are discussed. A quadrupole with added hexapole field can be constructed with round rods by rotating two rods (say the y rods) towards an x rod. Computer simulations are used to investigate the possibility of mass analysis with quadrupoles with added hexapole fields. We find that a quadrupole with an added hexapole field in the range 2–12% can provide mass analysis provided the dc is applied with the correct polarity and value. When a rod set is constructed with round rods, other multipoles in the potential degrade the peak shape, resolution and transmission. The largest of these after the quadrupole and hexapole are a dipole and octopole term. With round rod sets, the peak shape can be improved by using different diameters for the x and y rod pairs to minimize the octopole term in the potential and by injecting ions at the field center where the dipole term is zero. Calculations of the boundaries of the stability diagram for this case show the boundaries move out, relative to those of a pure quadrupole field, but remain sharp. (J Am Soc Mass Spectrom 2006, 17, 1063–1073) © 2006 American Society for Mass Spectrometry

Three dimensional Paul traps may benefit from distortions of their electrode geometry so that the electric potential is not described purely by a quadrupole field [1]. The distortions are described mathematically by the addition of higher multipoles (or spatial harmonics) to the potential. One effect of the higher multipoles is to cause the frequency of ion oscillation to shift with the amplitude of oscillation. It has been argued that this improves fragmentation efficiency in MS/MS because it becomes more difficult to eject ions from the trap, thus favoring ion activation and fragmentation over ion ejection [1]. An added positive even multipole can also lead to faster ion ejection at a stability boundary [1, 2] or with resonant excitation [3]. These benefits might also be expected to apply to a linear quadrupole trap.

Several studies have shown that the MS/MS efficiency (i.e., the fragmentation efficiency) of a linear quadrupole trap is improved by adding higher multipoles to the potential. Collings et al. [4] found surprisingly high MS/MS efficiency in a linear quadrupole operated at a pressure of 3.5×10^{-5} torr. This was attributed to the multipoles added to the potential by constructing the quadrupole with round rods. In a later study, Collings showed that the addition of a dc octopole to the potential with auxiliary electrodes could also increase the MS/MS efficiency [5]. An octopole field can be added to a linear quadrupole by constructing the quadrupole with one rod pair different in diameter from the other rod pair, or by using different spacings from the axis of equal diameter rod pairs [6]. Michaud et al. showed that a linear quadrupole with an added 4% octopole field can have substantially higher MS/MS efficiency than a conventional quadrupole rod set constructed from round rods, particularly at trap pressures of 10^{-4} torr or less of N_2 [7].

Frequency shifts can also be induced by the addition of a hexapole to a quadrupole potential, and addition of a hexapole should also increase MS/MS efficiency. The potential of a linear quadrupole with an added hexapole and no other multipoles is given by

Published online June 5, 2006

Address reprint requests to Dr. D. J. Douglas, Department of Chemistry, University of British Columbia, 2036 Main Mall, Vancouver, BC, V6T 1Z1, Canada. E-mail: douglas@chem.ubc.ca

* Current address: Department of Chemistry, Fudan University, Shanghai, China

1044-0305/06/$32.00
doi:10.1016/j.jasms.2006.03.013

Received February 10, 2006
Revised March 27, 2006
Accepted March 28, 2006

$$V(x,y,t) = \left[A_2\left(\frac{x^2-y^2}{r_0^{\,2}}\right) + A_3\left(\frac{x^3-3xy^2}{r_0^{\,3}}\right)\right]\varphi(t) \qquad (1)$$

where A_2 and A_3 are the dimensionless amplitudes of the quadrupole and hexapole fields, $A_2 \approx 1$, $r_0/\sqrt{A_2}$ is the distance from the center of the quadrupole to a y electrode when $x = 0$ and $\pm\varphi(t)$ is the voltage applied the electrodes. In this paper we describe the frequency shifts expected from the addition of a hexapole field within the effective potential model. Wells has shown that a hexapole term can be added to a linear quadrupole ion trap by applying dipole excitation at the frequency of the trapping rf [8]. The amplitude of the hexapole is determined by the dipole excitation voltage. We describe methods to construct a linear quadrupole with added hexapole field with exact electrode geometry. We also describe round rod geometries that add a hexapole field. We show that a quadrupole with added hexapole can be constructed with round rods by rotating two rods (say the y rods) towards an x rod. In some instruments it is desirable to have a linear quadrupole which can be operated as a trap with high MS/MS efficiency at pressures of ca. 10^{-5} torr but the same quadrupole must be capable of mass analysis with rf and dc voltages applied between the rods [9]. It has been found that linear quadrupoles with added octopole fields can perform mass analysis provided the dc potential is applied to the rods with the correct polarity [10]. Thus, we also use computer simulations to investigate the possibility of mass analysis with quadrupoles with added hexapole fields. We find that a quadrupole that has the potential given by eq 1 gives good peak shape and transmission in mass analysis provided the dc is applied with the correct polarity and value, but that when a rod set is constructed with round rods, other multipoles in the potential degrade the peak shape, resolution, and transmission. The largest of these after the quadrupole and hexapole are a dipole and octopole term. With round rod sets, the peak shape can be improved by using different diameters for the x and y rod pairs to minimize the octopole term in the potential and by injecting ions at the field center where the dipole term is zero. Calculations of the boundaries of the stability diagram for this case show the boundaries move out, relative to those of a pure quadrupole field, but remain sharp.

Methods

Multipole Calculations

In general a two-dimensional time-dependent electric potential can be expanded in multipoles as

$$V(x,y,t) = \varphi(t)\sum_{N=0}^{\infty} A_N\phi_N(x,y) \qquad (2)$$

where A_N is the dimensionless amplitude of the multipole $\phi_N(x,y)$, and $\varphi(t)$ is a time-dependent voltage applied to the electrodes [11]. For a quadrupole mass filter, $\phi(t) = U - V_{rf}\cos\Omega t$. Without loss of generality, for $N \geq 1$, $\phi_N(x,y)$ can be calculated from

$$\phi_N(x,y) = \mathrm{Re}\left[\frac{x+iy}{r_0}\right]^N \qquad (3)$$

where $\mathrm{Re}[(f(\zeta)]$ means the real part of the complex function $f(\zeta)$, $\zeta = x + iy$, and $i^2 = -1$. For rod sets with round rods, amplitudes of multipoles given by eq 3 were calculated with the method of effective charges [12].

Ion Source Model

Collisional cooling of ions in an RF quadrupole (or other multipole) has become a common method of coupling atmospheric pressure ion sources such as ESI to mass analyzers [13]. Collisions with background gas thermalize ions and concentrate ions near the quadrupole axis. We use an approximate model of a thermalized distribution of ions as the source for calculations of peak shapes and stability diagrams. At the input of the quadrupole, the ion spatial distribution is approximated as a Gaussian distribution with the probability density function f(x,y)

$$f(x,y) = \frac{1}{2\pi\sigma_x^{\,2}}e^{-\left(\frac{x^2+y^2}{2\sigma_x^{\,2}}\right)} \qquad (4)$$

where σ_x determines the spatial spread in both the x and y directions.

Modeling initial ion coordinates x and y with a random distribution given by eq 4 is based on the central limit theorem [14] for dimensionless variables $\tilde{x} = x/r_0$ and $\tilde{y} = y/r_0$ on the interval [-1, 1]. The distribution of eq 4 can be generated from

$$\tilde{x} = \sqrt{\frac{3}{m}}\,\sigma_x\sum_{i=1}^{m} x_i;\ \tilde{y} = \sqrt{\frac{3}{m}}\,\sigma_x\sum_{i=1}^{m} y_i \qquad (5)$$

where m is the number of random numbers x_i and y_i generated by a computer. In our calculations m = 100.

The ion velocities are taken from a thermal distribution given by

$$g(\nu_x,\nu_y) = \frac{1}{2\pi\sigma_\nu^{\,2}}e^{-\left(\frac{m(\nu_x^2+\nu_y^2)}{2kT}\right)} \qquad (6)$$

where $\sigma_\nu = \sqrt{\frac{2kT}{m}}$ is the ion velocity dispersion, k is Boltzmann's constant, T is the ion temperature, and m is the ion mass. Transverse velocities in the interval $[-3\sigma_v, 3\sigma_v]$ were used for every initial position. The dimensionless variables $\xi = \frac{\Omega t}{2}$ and $u = \frac{x}{r_0}$ are used in the ion motion equations. Then $\frac{du}{d\xi} = \frac{dx}{dt}\frac{1}{\pi r_0 f} = \frac{\nu}{\pi r_0 f}$ and $f = \frac{\Omega}{2\pi}$. The dimensionless velocity dispersion σ_u is

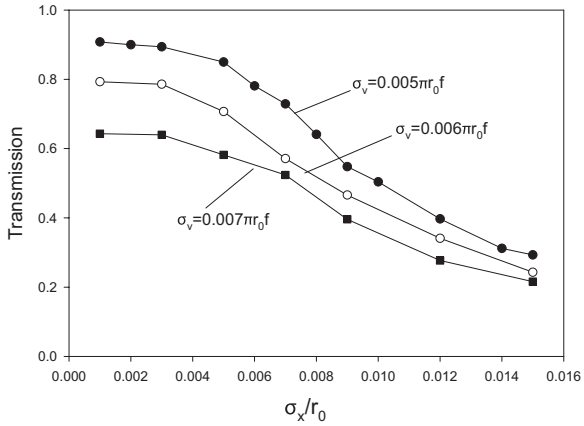

Figure 1. Transmission versus σ_x/r_0 for different values of transverse ion velocity dispersion σ_v with mass 390, 300K, R = 390, λ = 0.1676, and 150 rf cycles in the field.

$$\sigma_u = \frac{\sigma_v}{\pi r_0 f} = \frac{\sqrt{\frac{2kT}{m}}}{\pi r_0 f} \tag{7}$$

For typical conditions: an ion mass of 390 Da, $r_0 = 5 \times 10^{-3}$m, f = 1.0×10^6 Hz, and T = 300K, eq 7 gives $\sigma_u = \sigma_v/\pi r_0 f = 0.0072$. The ion velocity dispersion σ_v decreases with m as $m^{-1/2}$. This helps to improve the transmission of a quadrupole mass filter at higher mass.

The ion source model is characterized by the two parameters σ_x and σ_v. The influence of the radial size of the ion beam on transmission for different values σ_v is shown in Figure 1. These data were calculated for a resolution $q/\Delta q$ of the scan line of R = 390, λ = 0.1676 (λ is defined below), ion temperature T = 300 K, a separation time of n = 150 rf cycles, a pure quadrupole field and no fringing fields. With ions concentrated near the axis with $\sigma_x < 0.006r_0$ the transmission does not depend strongly on σ_x for given values of σ_v. For the same conditions the transmission for different values of σ_x are shown in Figure 2. High transmission, near 100% at m/z = 390, is possible because of the small ion beam emittance with $\sigma_x = 0.005r_0$ and $\sigma_v = 0.003\pi\ r_0 f$.

Peak Shape and Stability Region Calculations

Ion motion in quadrupole mass filters is described by the two Mathieu parameters a and q given by

$$a = \frac{8eU}{mr_0^2\Omega^2} \text{ and } q = \frac{4eV_{rf}}{mr_0^2\Omega^2} \tag{8}$$

where e is the charge on an ion, U is the DC applied from an electrode to ground and V_{rf} is the zero to peak rf voltage applied from an electrode to ground. For given applied voltages U and V_{rf}, ions of different mass to charge ratios lie on a scan line of slope

$$a/q = 2\lambda = \frac{2U}{V_{rf}} \tag{9}$$

The presence of higher order spatial harmonics in addition to the quadrupole field leads to changes in the stability diagram [10]. The detailed mathematical theory of the calculation of the stability boundaries for Mathieu and Hill equations is given in [15] and for mass spectrometry applications is reviewed in [16]. However these methods cannot be used when the x and y motions are coupled by higher spatial harmonics. Instead, the stability boundaries can be found by direct simulations of the ion motion. Details of these calculations of stability boundaries and peak shapes (i.e., the transmission versus q as the a and q parameters are varied along a scan line) are given in the Appendix part A.

Results

Frequency Shifts with an Added Hexapole Field

The frequency shifts that occur when a hexapole field is added to a linear quadrupole field can be calculated within the effective potential approximation [17], using the solution to the resulting nonlinear differential equation as described by Landau and Lifshitz [18]. Details of the calculation are in the Appendix Part B.

Ion motion in the x direction is determined by

$$\ddot{x} + \omega_0^2 x = -\frac{9eqA_2A_3}{4mr_0^3}V_{rf}x^2 - \frac{36eqA_3^2}{16mr_0^4}V_{rf}x^3 \tag{10}$$

where ω_0 is the secular frequency with no added multipole.

The frequency shift of the nonlinear oscillator described by eq 10 is

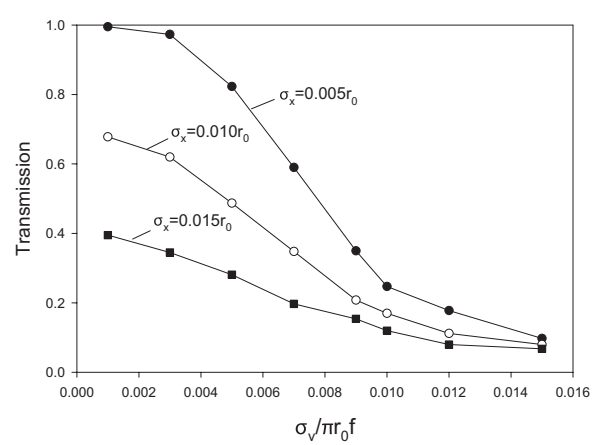

Figure 2. Transmission versus $\sigma_v/\pi r_0 f$ for three different spatial dispersions σ_x for the conditions of Figure 1.

$$\Delta\omega_x = -\frac{5}{12}\frac{81A_3^2}{4A_2^2}\frac{b^2}{r_0^2}\omega_0 + \frac{27}{16}\frac{A_3^2}{A_2^2}\frac{b^2}{r_0^2}\omega_0 \tag{11}$$

where b is the amplitude of oscillation. For example, if $A_3 = 0.02$ and $b = r_0$, the first term on the right of eq 11 gives a shift of $-3.38 \times 10^{-3}\ \omega_0$ and the second term a shift of $+6.75 \times 10^{-4}\ \omega_0$. The combined frequency shift for the x motion is $-2.71 \times 10^{-3}\ \omega_0$.

The motion in the y direction is determined by

$$\ddot{y} + \omega_0^2 = -\frac{36eqA_3^2}{16mr_0^4}V_{rf}\,y^3 \tag{12}$$

This gives a shift up in frequency

$$\Delta\omega_y = \frac{27A_3^2}{16A_2^2}\frac{b^2}{r_0^2}\omega_0 \tag{13}$$

When $A_2 = 1.0$, $A_3 = 0.020$ and $b = r_0$ this shift is $+6.75 \times 10^{-4}\omega_0$, opposite in sign and four times less than the total shift in the x frequency.

A hexapole produces smaller shifts than an octopole of the same amplitude. A positive octopole of amplitude A_4 in the x direction produces a shift in frequency of [7]

$$\Delta\omega_x = 3\frac{A_4}{A_2}\frac{b^2}{r_0^2}\omega_0 \tag{14}$$

If $A_4 = 0.02$ and $b = r_0$ this shift is $0.06\omega_0$ or about 22 times greater than that of a hexapole of the same amplitude. Nevertheless the frequency shift from a hexapole should be sufficient to improve MS/MS efficiency. Collings et al. [5] found that MS/MS efficiency for ions of a substituted triazatriphosphorine (mass to charge ratio $m/z = 2721.89$) was improved significantly under conditions where an added dc octopole field caused a shift of 0.4 kHz from the unperturbed frequency of 59.8 kHz ($\Delta\omega/\omega = 6.7 \times 10^{-3}$). From eq 11 this frequency shift could be caused by a ca. 3% hexapole field when $b = r_0$ or a ca. 6% hexapole field when $b = r_0/2$.

Methods to Add a Hexapole Field to a Linear Quadrupole

The rod shapes of linear quadrupoles with small amounts of added hexapole fields can be calculated from

$$A_2\left(\frac{x^2 - y^2}{r_0^2}\right) + A_3\left(\frac{x^3 - 3xy^2}{r_0^3}\right) = \pm c \tag{15}$$

where c is a constant. Taking $r_0 = 1$ and $c = 1$ gives

$$A_2(x^2 - y^2) + A_3(x^3 - 3xy^2) = \pm 1 \tag{16}$$

Eq 16 is quadratic in y and can be solved to give

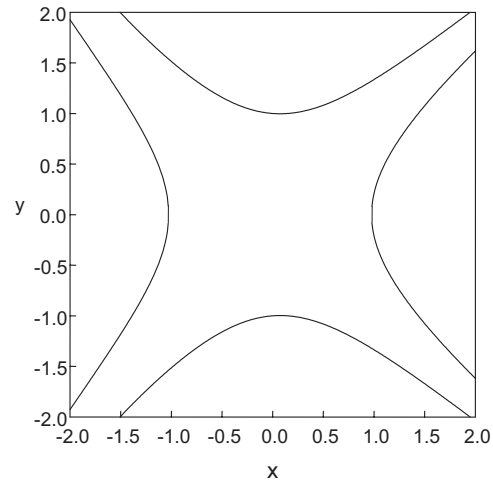

Figure 3. Cross sections of the electrodes that produce a linear quadrupole field of amplitude $A_2 = 1.0$ with an added hexapole field of amplitude $A_3 = 0.05$.

$$y = \pm\sqrt{\frac{A_3x^3 + A_2x^2 \mp 1}{3A_3x + A_2}} \tag{17}$$

Figure 3 shows the calculated shapes of the electrodes with $A_2 = 1.00$ and $A_3 = 0.05$. Electrodes with these exact shapes produce a quadrupole field with an added hexapole and no other multipoles in the potential. In this case other multipoles will only be produced by mechanical imperfections.

Eq 15 and Figure 3 show that with an added hexapole the rods sets are symmetric under the transformation $y \rightarrow -y$, but not under the transformation $x \rightarrow -x$. This contrasts to rod sets with added octopoles, which have fields and electrodes that are symmetric under both of these transformations. Eq. 15 shows that changing the sign of A_3 is equivalent to the transformation $x \rightarrow -x$. Rod sets constructed with a hexapole component A_3 and hexapole component $-A_3$ differ only by a reflection in the y axis. Physically, the same transformation can be achieved by rotating a rod set 180 degrees about its center to interchange the entrance and exit ends. This gives the same rod set with the same potentials applied to the x and y rod pairs. The character of ion trajectories and the performance of the rod set will not change. Thus, rod sets with $\pm A_3$ are equivalent. This contrasts with rod sets with added octopoles where changing the sign of A_4 is equivalent to interchanging the x and y rods. Because the x and y rods are physically different and have different applied potentials, changing the sign of A_4 changes the character of the ion trajectories [6, 7].

Constructing and mounting rod sets with the geometry shown in Figure 3 with high precision might be difficult and expensive. As with conventional quadrupole rod sets, it is advantageous if the field can be produced with sufficient accuracy with round rods. When round rods are used, an angular displacement of

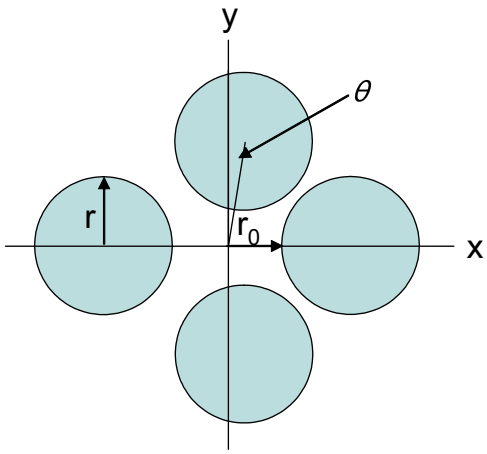

Figure 4. Electrode geometry for adding a hexapole field by rotating two *y* rods through an angle θ toward an *x* rod.

one rod produces an added hexapole field [12]. However the amplitudes of other multipoles are substantial. Examination of Figure 3 shows that the two y rods are closer to the x rod in the positive x direction. This suggests that, with round rods, a better approximation to the field might be achieved by rotating the two y rods toward one of the x rods, as shown in Figure 4. In Figure 4, all rods have the same diameter r and are equally spaced from the axis a distance r_0. The two y rods are rotated through an angle θ toward an x rod.

Figure 5 shows the multipole amplitudes A_1, A_3, A_4, A_5, and A_6 calculated for a ratio $r/r_0 = 1.1487$ and different angles of rotation, θ. This ratio r/r_0 was chosen because it makes the higher order multipole terms small when $\theta = 0$ [19]. The effects of small changes in r/r_0 when $\theta = 0$ have been reviewed by Douglas and Konenkov [20]. These amplitudes are shown because they are the largest produced with this rod geometry. It can be seen that a hexapole component is produced with amplitude approximately proportional to the rotation angle, given by $A_3 = 0.01545\theta$. At the same time

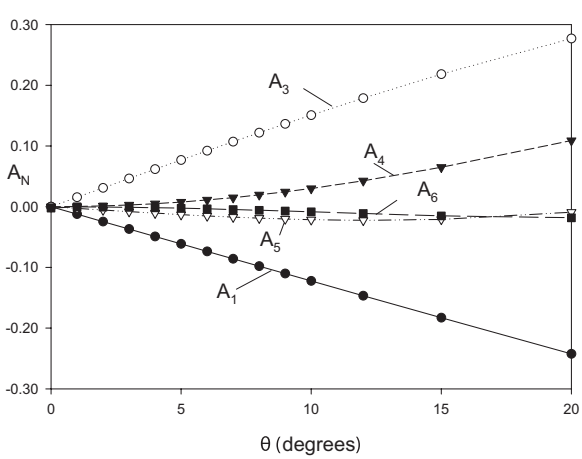

Figure 5. Multipole amplitudes, A_N versus rotation angle θ for a rod set with $r/r_0 = 1.1487$.

Table 1. Amplitudes of multipoles produced with round rods, $r/r_0 = 1.1487$ and a rotation angle of 3 degrees

Multipole	Amplitude
A_0	3.73×10^{-5}
A_1	-3.68×10^{-2}
A_2	1.0011
A_3	4.64×10^{-2}
A_4	2.77×10^{-3}
A_5	-8.18×10^{-3}
A_6	-1.098×10^{-3}
A_7	-1.43×10^{-3}
A_8	-1.54×10^{-4}
A_9	5.00×10^{-4}
A_{10}	-2.29×10^{-3}

a dipole component A_1 is produced. Other higher harmonics remain relatively small. Table 1, for example shows the harmonics produced with a rotation angle of 3.0°.

The Dipole Term A_1

Figure 5 and Table 1 show that with the geometry of Figure 4, there is a significant dipole term, A_1. (The dipole term in the potential has the form $A_1\left(\frac{x}{r_0}\right)\varphi(t)$.) This term arises because the field is no longer symmetric about the y axis. The dipole term can be removed by applying different voltages to the two x rods, either with a larger voltage applied to the x rod in the positive x direction or a smaller voltage applied to the x rod in the negative x direction, or a combination of these changes [21].

The dipole term arises because the center of the field is no longer at the point x = 0, y = 0 of Figure 4. The potential is approximately given by

$$V(x,y) = \left[A_1\left(\frac{x}{r_0}\right) + A_2\left(\frac{x^2-y^2}{r_0^2}\right) + A_3\left(\frac{x^3-3xy^2}{r_0^3}\right)\right]\varphi(t) \tag{18}$$

Let $\hat{x} = x + x_0$ or $x = \hat{x} - x_0$. Then

$$\frac{V(\hat{x},y)}{\varphi(t)} = A_1\left(\frac{(\hat{x}-x_0)}{r_0}\right) + A_2\left(\frac{(\hat{x}-x_0)^2-y^2}{r_0^2}\right) + A_3\left(\frac{(\hat{x}-x_0)^3-3(\hat{x}-x_0)y^2}{r_0^3}\right) \tag{19}$$

Expanding the terms gives

$$\frac{V(\hat{x},y)}{\varphi(t)} = A_3\left(\frac{\hat{x}^3}{r_0^3}\right) + \left(\frac{A_2}{r_0^2} - \frac{3x_0A_3}{r_0^3}\right)\hat{x}^2 + \left(\frac{A_1}{r_0} - \frac{2x_0A_2}{r_0^2} + \frac{3x_0^2A_3}{r_0^3} - \frac{3y^2}{r_0^3}\right)\hat{x}$$

Table 2. Comparison of values of x_0 from the approximate eq 23 and the exact eq 24

θ (degrees)	A_1	A_2	A_3	x_0 from eq 23	x_0 from eq 24
2.56	−0.0314	1.001	0.0396	$-0.0157r_0$	$-0.0156r_0$
5.13	−0.0629	0.9975	0.0789	$-0.0315r_0$	$-0.0313r_0$
7.69	−0.0942	0.9906	0.1172	$-0.0471r_0$	$-0.0467r_0$

$$+\left(\frac{-A_1x_0}{r_0}+\frac{A_2{x_0}^2}{{r_0}^2}-\frac{A_3{x_0}^2}{{r_0}^3}\right)$$

Consider the coefficient of $\hat{x}$ when $y = 0$. This will be zero if

$$\frac{A_1}{r_0}-\frac{2x_0A_2}{{r_0}^2}+\frac{3{x_0}^2A_3}{{r_0}^3}=0 \tag{21}$$

The last term is much smaller than the first two, so to a good approximation the coefficient of the dipole is zero if

$$\frac{A_1}{r_0}-\frac{2x_0A_2}{{r_0}^2}=0 \tag{22}$$

or

$$x_0=\frac{A_1r_0}{2A_2} \tag{23}$$

More exactly, eq 21, which is quadratic in x_0, can be solved to give

$$x_0=\frac{\frac{2A_2}{{r_0}^2}\pm\sqrt{\frac{4{A_2}^2}{{r_0}^2}-4\frac{A_1}{r_0}\frac{3A_3}{{r_0}^3}}}{2\frac{3A_3}{{r_0}^3}} \tag{24}$$

It is the solution with the minus sign that is realistic. Table 2 shows the approximate and exact values of x_0 calculated from eq 23 and eq 24 respectively for three rotation angles which give nominal hexapole fields of 4, 8, and 12%.

Because $A_1 < 0$, $x_0 < 0$. e.g., $\hat{x} = x - 0.0315r_0$. When $\hat{x} = 0$, $x = +0.0315r_0$. When $x = 0$, $\hat{x} = -0.0315r_0$. The center of the field is shifted in the direction of the positive x axis. This calculation is still approximate because it does not include the higher multipoles. However, it is likely adequate for practical purposes.

In the coordinate system centered on $\hat{x} = 0$, the multipoles differ somewhat from the multipoles shown in Figure 5 and Table 1. In the $\hat{x}$ coordinate system the coefficient of $\hat{x}^2$ is $\left(\frac{A_2}{{r_0}^2}-\frac{3x_0A_3}{{r_0}^3}\right)^2$. Using the simple form $x_0 \approx \frac{A_1r_0}{2}$, the term in $\hat{x}^2$ is

$$\left(A_2-\frac{\frac{3A_1A_3}{2}}{{r_0}^2}\right)\hat{x}^2 \tag{25}$$

where in eq 23 we have taken $A_2 = 1$; e.g., for an 8% hexapole ($\theta = 5.13°$), $A_1 = -0.0629$, $A_3 = 0.0789$, and the coefficient changes from $A_2 = 0.99738$ to $1.00 + 1.5(0.0629)(0.0789) = 1.0074$, a slight difference in the quadrupole term. Table 3 shows the multipoles for a rotation angle of $\theta = 3.85°$, (nominal 6% hexapole) in a coordinate system centered on $x = 0$, $y = 0$, and in the coordinate system centered on $\hat{x} = 0, y = 0$. First simulations of peak shapes and transmission with the thermalized ion source and a coordinate system centered on x = 0, y = 0 including the dipole term, showed very low transmission. When the dipole term was not included, the transmission increased significantly. Therefore all the calculations of peak shapes and transmission for round rod sets shown below were done with multipoles calculated for the co-ordinate system that makes the dipole term zero. Experimentally this can be done by injecting the ions at the point $\hat{x} = 0, y = 0$.

Mass Analysis

The addition of higher multipoles to a linear quadrupole operated as a mass filter has generally been considered undesirable [22]. Nevertheless it has recently been shown that linear quadrupoles with substantial added octopole fields ($A_4 = 0.02 - 0.04$) can in fact be operated as mass filters [6]. This led us to investigate the possibility of using quadrupoles with added hexapole fields as mass filters.

Table 3. Multipole amplitudes in a co-ordinate system centered on x = 0, y = 0, and in a coordinate system that makes $A_1 = 0$ with $r/r_0 = 1.1487$, and $\theta = 3.85$ degrees

Multipole	Amplitude (x = 0, y = 0)	Amplitude $\hat{x}$ = 0, y = 0
A_0	6.15×10^{-5}	-4.89×10^{-4}
A_1	-4.72×10^{-2}	0.000
A_2	0.9999	1.004
A_3	5.94×10^{-2}	5.98×10^{-2}
A_4	4.56×10^{-3}	3.32×10^{-3}
A_5	-1.04×10^{-2}	-1.06×10^{-2}
A_6	-1.64×10^{-3}	-1.96×10^{-3}
A_7	-1.89×10^{-3}	-1.9310^{-3}
A_8	-2.60×10^{-4}	-1.83×10^{-4}
A_9	6.28×10^{-4}	9.1×10^{-4}
A_{10}	-2.18×10^{-3}	-2.37×10^{-3}

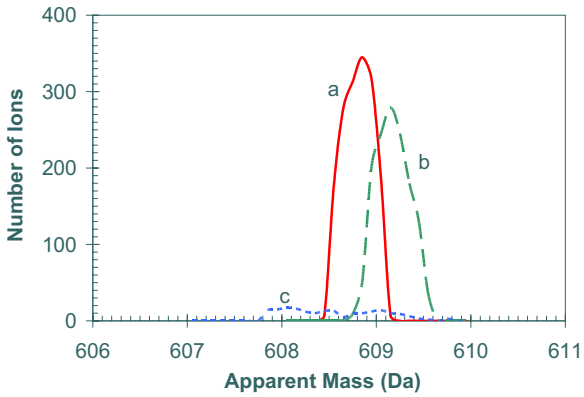

Figure 6. Peak shapes obtained (**a**) with a pure quadrupole field, $\lambda = 1.667$ (**b**) with a quadrupole field with 2% added hexapole, and $\lambda = +0.1680$ (**c**) with a quadrupole field with 2% added hexapole and $\lambda = -0.1665$.

Figure 6 shows calculated peak shapes for positive ions. Curve "a" shows a peak shape calculated for a pure quadrupole field and $\lambda = +0.1667$. For the simulations of Figure 6, 10,000 ions were uniformly distributed over a circular aperture of radius 0.1 mm ($0.024r_0$) with thermal (300 K) radial speeds. Ions of $m/z = 609$ were injected into a 200 mm long quadrupole with an additional 1.0 eV of energy (speed 561 m s^{-1}, 356 cycles in the 1.0 MHz field). The ions were distributed randomly and uniformly along a scan line of nominal resolution 1000, corresponding to masses of 608.2 to 610.2. The peak from the pure quadrupole field shows a peak width at half height of $\Delta m/z = 0.53$ ($R_{1/2} = 1150$). Figure 6 curve b shows the peak shape obtained when a 2% hexapole ($A_3 = 0.02$) is added to the quadrupole potential, and the positive dc is applied to the x rods and the negative dc to the y rods. Higher multipoles are not included in the calculation; the potential is given by eq 1. Preliminary results had shown that with an added hexapole a broader peak with lower resolution is obtained in comparison to a pure quadrupole operated at the same value of λ. For curve b, λ was increased to 0.1680 to give a peak shape with resolution comparable to that of the pure quadrupole field. This scan line does not intersect the tip of the stability region of a pure quadrupole field. Figure 6 shows when there is a 2% hexapole field and $\lambda = 0.1680$ the resolution ($R_{1/2} = 1130$) and peak shape are comparable to those of a pure quadrupole field. Curve c shows the peak shape and transmission when the polarity of the dc is reversed (positive dc on the y rods and negative dc on the x rods). For this calculation the magnitude of λ was lowered to 0.1665 in an attempt to increase the transmission. The peak is broad and the transmission is very low. Thus mass analysis is possible with a quadrupole field with added hexapole field but the dc must be applied with the correct polarity. This is analogous to mass analysis with an added octopole field [10].

Figure 7a shows peak shapes for quadrupoles with 2, 8, and 12% added hexapole fields, with $\lambda = 0.1676$. With increasing amounts of hexapole the peak broadens but remains smooth with sharp sides. The broadening results from changes to the stability diagram described below. As the amplitude of the hexapole increases, the transmission increases. Figure 7b shows peak shapes with 2, 8, and 12% added hexapole field and with λ increased to increase the resolution. The resolution with a 2% hexapole field is ca. 1800, with 8% hexapole 300, and with 12% hexapole 180.

Peak Shapes with Round-Rod Sets

The simulations of Figures 6 and 7 include no multipoles higher than the hexapole. When round rods are used as in Figure 4, other multipoles are added to the field. Figure 8 shows peak shapes calculated for quadrupoles constructed with round rods. For this calculation all the multipoles up to $N = 10$ in the coordinate system that makes $A_1 = 0$ were included. As the hexapole component increases, the transmission decreases, and the resolution drops from $R_{1/2} = 370$ when $A_3 = 0.02$ to $R_{1/2} = 300$ when $A_3 = 0.12$. The transmission with $A_3 = 0.12$ drops from nearly 100% (Figure 7a) to less than 10%. In addition, there is undesirable

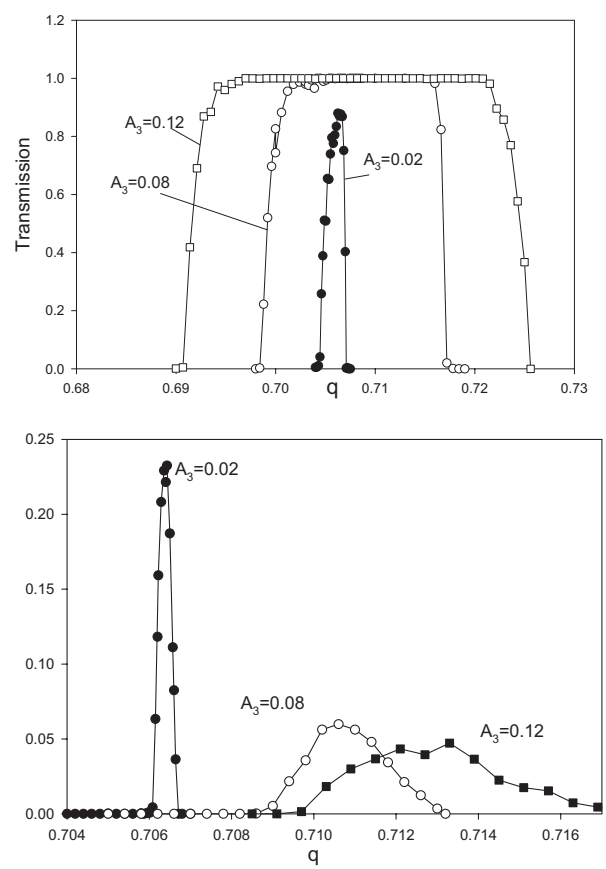

Figure 7. (**a**) Peak shapes for a quadrupole field with added hexapole components of 2, 8, and 12% with $\sigma_x = 0.002r_0$, $\sigma_v = 0.007$, $\lambda = 0.1676$ and 100 cycles in the field (**b**) at higher resolution and with 150 cycles in the field. With $A_3 = 0.02$, $\lambda = 0.1680$, with $A_3 = 0.08$, $\lambda = 0.1706$ and with $A_3 = 0.12$, $\lambda = 0.1730$.

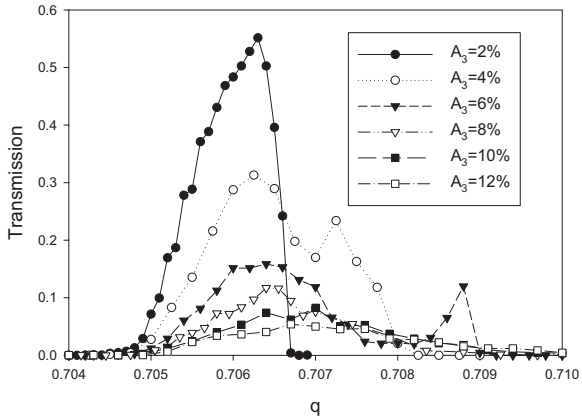

Figure 8. Peak shapes with $r/r_0 = 1.1487$ and round rods with nominal hexapole components of 2, 4, 6, 8, 10, and 12%, with $\sigma_x = 0.002r_0$, $\sigma_v = 0.007$, $\lambda = 0.1676$, 150 rf cycles in the field and $\lambda = 0.1676$.

structure on the peak. Clearly, the higher multipoles affect the transmission and resolution.

Peak Shapes with $A_4 \approx 0$.

After A_1 and A_3, the next highest term in the multipole expansion is the octopole term (Figure 5). This term can be minimized by constructing the rod sets with different diameters for the x and y rods. For a given rotation angle, the diameter of the x rods, r_x, can be increased to make $A_4 \approx 0$. These diameters are shown in Table 4. When A_4 is minimized, the peak shape improves. Figure 9a shows peak shapes calculated with $\lambda = 0.1676$ and the geometries that minimize A_4. In comparison to round rod sets with $A_4 \neq 0$ (Figure 8) the transmission is greatly improved. At these low resolutions the peak shapes are similar to those of a quadrupole with a pure added hexapole only (Figure 7a). When λ is increased, the resolution increases. Figure 9b shows peak shapes with nominal hexapole components of 6, 8, 10, and 12%, and with scan lines chosen to give increased resolution. At both low (Figure 9a) and high-resolution (Figure 9b) there is improved peak shape and transmission. In Figure 9b the peak for the 6% added hexapole shows the highest resolution with $R_{1/2} \approx 1400$. The other peaks have $R_{1/2} \approx 700–800$. The peaks with 8 and 12% hexapole show higher resolution and peak shapes free of structure in comparison to rod sets with the same hexapole amplitudes constructed with equal diameter rods (Figure 8). The peaks

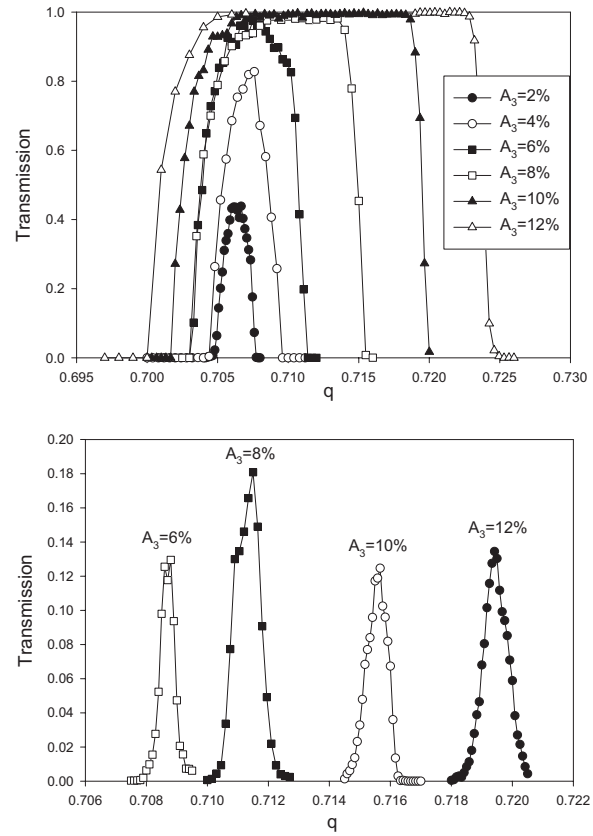

Figure 9. (**a**) Peak shapes with round rods, and r_x/r_0 chosen to minimize A_4, calculated with $A_1 = 0$ and with $\sigma_x = 0.002r_0$, $\sigma_v = 0.007$, $\lambda = 0.1676$ and 150 rf cycles in the field. (**b**) peak shapes with $A_1 = 0$ and $A_4 \approx 0$ at higher resolution with rod sets with added hexapole fields of 6, 8, 10, and 12% operated at $\lambda = 0.16857$, $\lambda = 0.1692$, $\lambda = 0.1705$, and $\lambda = 0.1715$, respectively.

with 8 and 12% hexapole also have higher transmission and resolution than a quadrupole with only an added hexapole of the same amplitude (Figure 7b). Thus making $A_4 = 0$ improves the peak shape. However at intermediate resolution there can still be structure of the peaks. This is illustrated in Figure 10, which shows peak shapes for a quadrupole with nominally 10% hexapole and $A_4 \approx 0$. The two peaks with $\lambda = 0.17000$ and $\lambda = 0.17015$ with intermediate resolution have dips on the low mass side.

Stability Diagrams

Adding a hexapole field to a linear quadrupole causes the stability boundaries to shift. Calculated stability

Table 4. Values of r_x/r_0 that give $A_4 \approx 0$

Nominal A_3	Angle (degrees)	A_3	A_4	New r_x/r_0 to make $A_4 = 0$	A_4 with new r_x
2%	1.28	0.0198299	0.0005060	1.1540	5.62×10^{-5}
4%	2.56	0.0396057	0.0020210	1.1730	1.38×10^{-5}
6%	3.85	0.0594268	0.0045593	1.2050	5.05×10^{-6}
8%	5.13	0.0789318	0.0080662	1.2500	2.51×10^{-5}
10%	6.50	0.0099569	0.0128860	1.3185	3.54×10^{-6}
12%	7.69	0.1172451	0.0179422	1.4000	1.75×10^{-4}

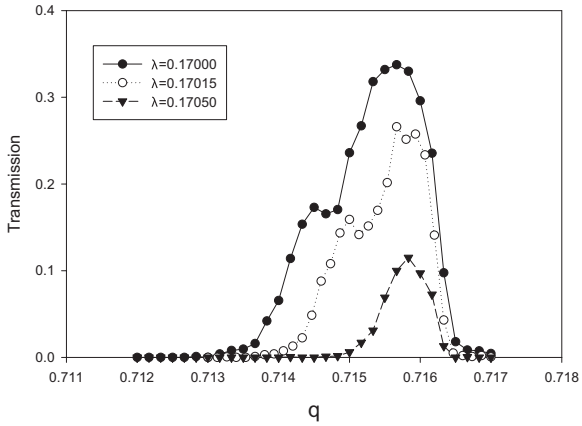

Figure 10. Peaks shape with a quadrupole with $\theta = 6.5°$, $A_3 = 0.1016$, $r_x/r_0 = 1.2672$. $r_y/r_0 = 1.1487$ calculated with $\sigma_x = 0.002$, $\sigma_v = 0.007$, and 150 cycles in the field.

boundaries for $a > 0$ (positive dc applied to the x rods and positive ions) are shown in Figure 11. The lines labeled 1 are the boundaries for an ideal quadrupole field. Line 2 shows the x boundary for a field with a quadrupole ($A_2 = 1.00$) and hexapole ($A_3 = 0.02$) but no other multipoles. The hexapole harmonic leads to a shift of the x boundary along the q axis, parallel to the original boundary. The addition of higher order spatial harmonics created by round rods gives additional shifts to the x boundary. Curve 3 shows the x boundary calculated for a rod set with nominal 2% hexapole field including the harmonics up to $N = 10$. Curves 4, 5, 6, 7, and 8 correspond to boundaries of rod sets constructed from round rods and with added hexapoles of 4, 6, 8, 10, and 12% created by round rods including the harmonics up to $N = 10$. For the calculations of boundaries 3–8 the multipole amplitudes of round rod sets that minimize A_4 were used, and the coordinate system that makes $A_1 = 0$ was used. Increasing the amplitude A_3 leads to strong shifts of the x boundary and an increased area of the stability regions. These shifts explain the increases in peak widths for a constant λ as the hexapole component increases. (Figures 7a, 8, 9a). They also explain the need for using higher values of λ as the hexapole amplitude increases (Figure 9b) and the shift of peaks to higher q values as the hexapole component increases (Figure 9b). With an added hexapole field, the tip of the stability region develops a "flat" boundary. This flat boundary is apparently sufficiently sharp to permit mass analysis. Attempts were made to calculate the stability diagram when $a < 0$ (negative dc applied to the x rods, positive ions). Only a diffuse region of stability with very low transmission was found. This is consistent with the low transmission and poor resolution of curve c in Figure 6.

The x boundary shows the greatest shift because it is the electric field in the x direction that changes the most with an added hexapole. Using eq 1, the electric fields are given by

$$E_x = -\frac{\partial V(x,y)}{\partial x} = \left[-\frac{2A_2}{r_0^2}x - \frac{3A_3}{r_0^3}x^2 + \frac{3A_3}{r_0^3}y^2\right]\varphi(t) \tag{26}$$

$$E_y = -\frac{\partial V(x,y)}{\partial y} = \left[\frac{2A_2}{r_0^2}y + \frac{6A_3}{r_0^3}xy\right]\varphi(t) \tag{27}$$

Considering the x direction when $y = 0$ and the y direction when $x = 0$ eq 26 and 27 can be written as

$$E_x = \left[-\frac{2A_2}{r_0^2}x\left[1 + \frac{3A_3}{2A_2 r_0}x\right]\right]\varphi(t) \tag{28}$$

$$E_y = \left[\frac{2A_2}{r_0^2}y\right]\varphi(t) \tag{29}$$

Eqs 28 and 29 show that the x electric field depends on the amplitude A_3 and that the y electric field is unchanged. This is approximate because the coupling of the x and y motion is not included in eqs 28 and 29.

Conclusions

A hexapole field about 1–10% of the quadrupole field can be added to a linear ion trap by constructing the electrodes with exact geometries or by using round rods with the two y rods rotated towards an x rod. Calculations of the frequency shifts caused by these fields suggest they should be sufficient to improve the fragmentation efficiency in MS/MS. If the same rod set is to be used for mass analysis, the best performance would seem to come from rod sets constructed with round rods where the x rods are increased in diameter to make the octopole term in the potential small, and with injection of the ions on the field center where the dipole

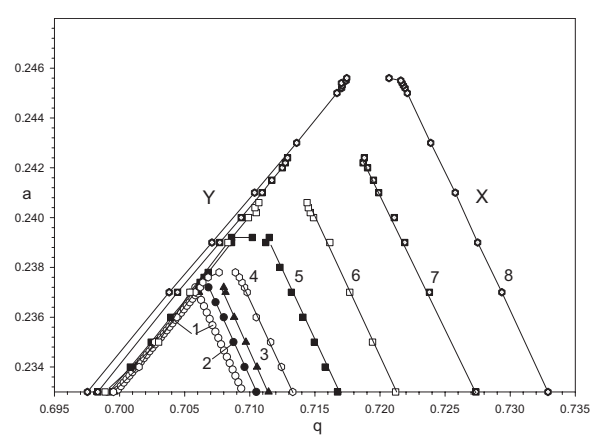

Figure 11. Stability boundaries calculated for 1% transmission with 150 rf cycles in the field (1) for a pure quadrupole field (2) for a quadrupole with 2% hexapole but no other multipoles, and for rod sets constructed with round rods that minimize A_4, calculated with $A_1 = 0$, for (3) 2% hexapole (4) 4% hexapole (5) 6% hexapole (6) 8% hexapole (7) 10% hexapole, and (8) 12% hexapole.

term is zero. Simulations of the stability diagram for these rod sets show that the stability boundaries move out but remain sharp provided the positive dc potential is applied to the x rods (for positive ions). Further optimization will be required to find the ratio for the y rod radius, r_y/r_0, for these rod sets that produces the best performance in mass analysis. All these results from computer simulations will require experimental confirmation, but they suggest that a linear trap with improved MS/MS efficiency and the capability of performing mass analysis will be possible when a hexapole field is added to a linear quadrupole field. Other combinations of quadrupole and multipole fields that can provide mass analysis remain to be explored.

Acknowledgments

This work was supported by the Natural Sciences and Engineering Research Council and MDS SCIEX through an Industrial Research Chair.

Appendix

A. Calculations of Peak Shapes and Stability Diagrams

With higher multipoles in the potential, ion motion is determined by [20]

$$\frac{d^2x}{d\xi^2} + \left[a + 2q\cos 2(\xi - \xi_0)\right]x = -\frac{1}{2} \times \left[a + 2q\cos 2(\xi - \xi_0)\right]\sum_{N=3}^{10} \frac{A_N \frac{\partial \phi_N}{\partial x}}{A_2^{N2} r_0^{N-2}} \quad \text{(A1)}$$

$$\frac{d^2y}{d\xi^2} - \left[a + 2q\cos 2(\xi - \xi_0)\right]y = -\frac{1}{2} \times \left[a + 2q\cos 2(\xi - \xi_0)\right]\sum_{N=3}^{10} \frac{A_N \frac{\partial \phi_N}{\partial y}}{A_2^{N2} r_0^{N-2}} \quad \text{(A2)}$$

Eqs A1 and A2 were solved by the Runge-Kutta—Nystrom—Dormand-Prince (RK-N-DP) method [23] and multipoles up to $N = 10$ were included. With the ion source model described above, N ion trajectories were calculated for fixed rf phases $\xi_0 = 0, \pi/20, 2*\pi/20, 3*\pi/20, \ldots, 19*\pi/20$. If a given ion trajectory is not stable (x or $y \geq r_0$) in the time interval $0 < \xi < n\pi$, where n is the number of rf cycles which the ions spend in the quadrupole field, the program starts calculating a new trajectory. From the number of transmitted ions, N_t, at a given point (a,q) the transmission is $T = N_t/N$. For both peak shape and stability boundary calculations, the number of ion trajectories, N, was 6000 or more at each point of a transmission curve. For the calculation of peak shapes, the values of a and q were systematically changed on a scan line with a fixed ratio λ. For the calculation of stability boundaries, a was fixed and q was systematically varied to produce a curve of transmission versus q. The true boundaries correspond to $n \to \infty$. For a practical calculation we choose $n = 150$ and the 1% level of transmission.

B. Calculation of the Frequency Shift with an Added Hexapole Field

For an ion of mass, m and charge, e, in an inhomogeneous electric field, $\vec{E}$, oscillating at angular frequency Ω, the effective electric potential [17] is given by

$$V_{eff} = \frac{e\left|\vec{E}\right|^2}{4m\Omega^2} \quad \text{(A3)}$$

where

$$\left|\vec{E}\right|^2 = \left(E_x^2 + E_y^2 + E_z^2\right) \quad \text{(A4)}$$

For the potential of eq 1 when $\phi(t) = V_{rf}\cos\Omega t$ eq A3 and A4 lead to

$$V_{eff}(x, y) = \frac{qA_2^2x^2}{4r_0^2}V_{rf} + \frac{3qA_2A_3x^3}{4r_0^3}V_{rf} + \frac{9qA_3^2x^4}{16r_0^4}V_{rf} + \frac{qA_2^2y^2}{4r_0^2}V_{rf} + \frac{9qA_3^2y^4}{16r_0^4}V_{rf} + \ldots \quad \text{(A5)}$$

Higher order terms in $x^m\ y^n$ have not been included because we are interested in the x motion when $y = 0$, and the y motion when $x = 0$. To first-order in A_3, the hexapole does not cause a shift in the frequency of oscillation because, while the potential increases more rapidly than that of a harmonic oscillator in the positive x direction, it increases less rapidly in the negative x direction. However, in second-order it does cause a frequency shift. Motion in the x direction in the effective potential of eq A5 is determined by

$$m\ddot{x} = F_x = -e\frac{\partial V_{eff}(x, y)}{\partial x} \quad \text{(A6)}$$

which leads to

$$\ddot{x} + \omega_0^2 x = -\frac{9eqA_2A_3}{4mr_0^3}V_{rf}x^2 - \frac{36eqA_3^2}{16mr_0^4}V_{rf}x^3 \quad \text{(A7)}$$

with

$$\omega_0^2 = \frac{eqA_2^2V_{rf}2}{4mr_0^2} \quad \text{(A8)}$$

or

$$\omega_0 = \frac{qA_2}{\sqrt{8}}\Omega \tag{A9}$$

The left side of eq A7 describes the secular motion of an ion trapped in a quadrupole field at low q values and the right side describes the modifications caused by the hexapole fields. Eq A7 is of the form

$$\ddot{x} + \omega_0{}^2 x = -\alpha x^2 - \beta x^3 \tag{A10}$$

with

$$\alpha = \frac{9}{2}\left(\frac{A_3}{A_2}\right)\frac{\omega_0{}^2}{r_0} \text{ and } \beta = \frac{9A_3^2}{2A_2^2}\frac{\omega_0{}^2}{r_0{}^2} \tag{A11}$$

The solution of eq A10 has been described by Landau and Lifshitz [18]. The terms on the right of eq A10 cause a shift in the frequency of ion oscillation given by

$$\Delta\omega = \left(\frac{3\beta}{8\omega_0} - \frac{5\alpha^2}{12\omega_0^3}\right)b^2 \tag{A12}$$

where b is the amplitude of oscillation. Thus the term in α in eq A10 causes a shift down in frequency of

$$\Delta\omega_\alpha = -\frac{5}{12}\frac{81A_3^2}{4A_2^2}\frac{b^2}{r_0^2}\omega_0 \tag{A13}$$

This shift was calculated by Sevugarajan and Menon [24] for the z motion in a 3D trap with an added hexapole field. The term in β in eq A10 causes a shift up of

$$\Delta\omega_\beta = +\frac{3\beta}{8\omega_0}b^2 = +\frac{27A_3^2}{16A_2^2}\frac{b^2}{r_0^2}\omega_0 \tag{A14}$$

For example, if $A_3 = 0.02$ and $b = r_0$, $\Delta\omega_a = -3.38 \times 10^{-3}\ \omega_0$ and $\Delta\omega_\beta = +6.75 \times 10^{-4}\ \omega_0$. The combined frequency shift for the x motion ($\Delta\omega_x = \Delta\omega_a + \Delta\omega_\beta$) is $-2.71 \times 10^{-3}\ \omega_0$.

References

1. Franzen, J.; Gabling, R.-H.; Schubert, M.; Wang, Y. Nonlinear Ion Traps. In *Practical Aspects of Ion Trap Mass Spectrometry*; Vol. V1; March, R. E.; Todd, J. F. J., Eds.; CRC Press: Boca Raton, 1995; pp 49–167.
2. Sudakov, M. Effective Potential and the Ion Axial Beat Motion Near the Boundary of the First Stable Region in a Nonlinear Ion Trap. *Int. J. Mass Spectrom.* **2001,** *206,* 27–43.
3. Makarov, A. A. Resonance Ejection from the Paul Trap: A Theoretical Treatment Incorporating a Weak Octapole Field. *Anal. Chem.* **1996,** *68,* 4257–4263.
4. Collings, B. A.; Stott, W. R.; Londry, F. A. Resonant Excitation in a Low Pressure Linear Ion Trap. *J. Am. Soc. Mass Spectrom.* **2003,** *14,* 622–634.
5. Collings, B. A. Increased Fragmentation Efficiency of Ions in a Low Pressure Linear Ion Trap with an Added dc Octopole Field. *J. Am. Soc. Mass Spectrom.* **2005,** *16,* 1342–1352.
6. Sudakov, M.; Douglas, D. J. Linear Quadrupoles with Added Octopole Fields. *Rapid Commun. Mass Spectrom.* **2003,** *17,* 2290–2294.
7. Michaud, A. L.; Frank, A. J.; Ding, C.; Zhao, X.; Douglas, D. J. Ion Excitation in a Linear Quadrupole Ion Trap with an Added Octopole Field. *J. Am. Soc. Mass Spectrom.* **2005,** *16,* 835–849.
8. Wells, G. J. Linear Ion Trap Apparatus and Method Utilizing an Asymmetrical Trapping Field. US Patent Application 2005/0263696, published December 1, 2005.
9. Hager, J. W. A New Linear Ion Trap Mass Spectrometer. *Rapid Commun. Mass Spectrom.* **2002,** *16,* 512–526.
10. Ding, C.; Konenkov, N. V.; Douglas, D. J. Quadrupole Mass Filters with Octopole Fields. *Rapid Commun. Mass Spectrom.* **2003,** *17,* 2495–2502.
11. Smythe, W. R. *Static and Dynamic Electricity*; McGraw-Hill Book Company: New York, 1939; pp 62–65.
12. Douglas, D. J.; Glebova, T.; Konenkov, N.; Sudakov, M. Y. Spatial Harmonics of the Field in a Quadrupole Mass Filter with Circular Electrodes. *Zh. Tekh. Fiz.* **1999**, *69*, 96–101.
13. (a) Douglas, D. J.; French, J. B. Collisional Focusing Effects in Radio Frequency Quadrupoles. *J. Am. Soc. Mass Spectrom.* **1992**, *3*, 398–408; (b) Douglas, D. J.; Frank, A. J.; Mao, D. Linear Ion Traps in Mass Spectrometry. *Mass Spec. Rev.* **2005**, *24*, 1–29.
14. Venttsel E. S. *Probability Theory. First Steps*; Mir Publishers: Moscow, 1982; p 79.
15. McLachlan, N. W. *Theory and Applications of Mathieu Functions*; Oxford University Press: London, UK, 1947; pp 10-56.
16. Konenkov, N. V.; Sudakov, M. Yu.; Douglas D. J. Matrix Methods for the Calculation of Stability Diagrams in Quadrupole Mass Spectrometry. *J. Am. Soc. Mass Spectrom.* **2002,** *13,* 597–613.
17. (a) Dehmelt, H. G. Radiofrequency Spectroscopy of Stored Ions, 1: Storage. *Adv. Atom. Mol. Phys.* **1967**, *3*, 53–72; (b) Gerlich, D. *Advances in Chemical Physics*; LXXXII *Inhomogeneous RF Fields: A Versatile Tool for the Study of Processes with Slow Ions*; John Wiley and Sons: New York, 1992; pp 1–176.
18. Landau, L. D.; Lifshitz, E. M. *Mechanics*, 3rd ed; Pergamon Press: New York, 1960; pp 74–93.
19. March, R. E.; Hughes, R. J. *Quadrupole Storage Mass Spectrometry*; John Wiley and Sons: Toronto, 1989; p 42.
20. Douglas, D. J.; Konenkov, N. V. Influence of the 6th and 10th Spatial Harmonics on the Peak Shape of a Quadrupole Mass Filter with Round Rods. *Rapid Commun. Mass Spectrom.* **2002,** *16,* 1425–1431.
21. Douglas, D. J., Ding, C-F., Londry, F. Method and Apparatus For Providing Two-Dimensional Substantially Quadrupole Fields Having Selected Hexapole Components. U.S. Patent Application 2005/0067564, published March 31, 2005.
22. (a) Dawson, P. H.; Whetton, N. R. Nonlinear Resonances in Quadrupole Mass Spectrometers Due to Imperfect Fields. *Int. J. Mass Spectrom. Ion Phys.* **1969**, *3*, 1–12; (b) Dawson. P. H. Ion Optical Properties of Quadrupole Mass Filters. *Adv. Elect. Electron. Optics* **1980**, *53*, 152–208.
23. Hairer, E.; Norsett, S. P.; Wanner, G. *Solving Ordinary Differential Equations*; Springer-Verlag: New York/Berlin, 1980; p 447.
24. Sevugarajan, S.; Menon, A. G. Field Imperfection Induced Axial Secular Frequency Shifts in Nonlinear Ion Traps. *Int. J. Mass Spectrom.* **1999,** *189,* 53–61.